DUST MORPHOLOGY AND COMPOSITION IN FU ORIONIS SYSTEMS

E. F. Polomski[1,2] and Charles E. Woodward
Department of Astronomy, University of Minnesota, 116 Church Street, SE, Minneapolis, MN 55455;
elwood@astro.umn.edu, chelsea@astro.umn.edu

Elizabeth K. Holmes[3]
Jet Propulsion Laboratory, Mail Stop 169-506, California Institute of Technology, 480 Oak Grove Drive, Pasadena, CA 91109;
holmes@jpl.nasa.gov

Harold M. Butner
Submillimeter Telescope Observatory, Steward Observatory, University of Arizona, Tucson, AZ 85721;
hbutner@jach.hawaii.edu

David K. Lynch[2] and Ray W. Russell[2]
Space Science Applications Laboratory, The Aerospace Corporation, P.O. Box 92957, Los Angeles, CA 90009;
david.k.lynch@aero.org, ray.w.russell@aero.org

Michael L. Sitko[2]
Department of Physics, University of Cincinnati, 400 Geology, Physics Building, Cincinnati, OH 45221-0011;
sitko@physics.uc.edu

Diane H. Wooden
NASA Ames Research Center, Mail Stop 245-1, Space Science Division, Moffet Field, CA 94035;
wooden@delphinus.arc.nasa.gov

and

C. M. Telesco[2] and R. Piña[2,4]
Department of Astronomy, University of Florida, Gainesville, FL 32611-2055; telesco@astro.ufl.edu
Received 2003 December 13; accepted 2004 October 20

ABSTRACT

FU Orionis stars are a small group of pre–main-sequence stars known for large-amplitude optical variability. These objects also exhibit multiwavelength phenomena suggestive of active accretion from a circumstellar disk. We present high spatial resolution mid-IR imaging and spectroscopy, submillimeter photometry, and 3–4 μm photometry of four FU Ori–class objects, RNO 1B and C, Z CMa, and Par 21, and one object classified as a pre–FU Ori star, V380 Ori. We resolve multiple IR sources and extended emission in the RNO 1B/C system, and we discuss in detail their association with disk activity and the source of the *Infrared Astronomical Satellite* far-IR and radio maser emission in this field. We derive dust temperatures and masses for all sources and discuss how dust composition and morphology is related to the evolutionary stage of these objects.

Key words: infrared: stars — planetary systems: protoplanetary disks — stars: pre–main-sequence

1. INTRODUCTION

The FU Orionis stars were first recognized as a distinct class of objects by Herbig (1966, 1977). The defining member of the class, FU Ori, was discovered by Wachmann (1939) when it exhibited a large optical outburst of as much as 5 mag. Later studies by Herbig (1966) found that FU Ori was located in a star-forming region and exhibited a spectrum similar to that of T Tauri stars. Higher spectral resolution observations revealed doubled absorption lines and line widths that declined toward longer wavelengths (Hartmann & Kenyon 1996). These phenomena have been interpreted as the signature of a kinematically rotating accretion disk around a pre–main-sequence

(PMS) star. An FU Ori outburst occurs when material in the dusty circumstellar disk is rapidly accreted onto the young star. During these outbursts, lasting up to tens of years, the accretion disk luminosity may exceed that of the central star by as much as a factor of 100 (Hartmann & Kenyon 1996). These episodic accretion events are assumed to occupy a brief phase of the disk+star evolution, after which the system evolves toward a more quiescent state (Weintraub et al. 1991). Approximately 19 FU Ori objects have now been identified (Sandell & Weintraub 2001). The phenomena associated with this class include F or G spectral types, optical outbursts, molecular outflows, broad CO absorption at 2.3 μm from a circumstellar disk, and prominent IR excesses.

The IR excesses of FU Ori objects have provided evidence for the presence of circumstellar accretion disks. Lada (1987) and Greene et al. (1994) defined a 2–20 μm PMS spectral energy distribution (SED) index, $\alpha = d \log(\lambda F_\lambda)/d \log \lambda$, which is linked to the spectral shape of the IR excess and the evolutionary stage and morphology of the circumstellar environment. In their scheme the youngest and most embedded objects are Class I sources, characterized by massive envelopes of gas and

---

TABLE 1
OSCIR Observing Log

	N			18 μm		
Object	UT Date	Telescope	Integration (s)	UT Date	Telescope	Integration (s)
RNO 1..................	1999 Nov 11	IRTF	192	1999 Nov 11	IRTF	112
RNO 1B/C	1999 Nov 11	IRTF	192	1999 Nov 11	IRTF	192
RNO 1B/C	. . .	. . .	. . .	1999 Nov 12	IRTF	368
V380 Ori..............	1998 Nov 29	CTIO	125	1998 Nov 29	CTIO	125
Z CMa..................	1998 Nov 29	CTIO	62	1998 Nov 29	CTIO	62
Z CMa..................	1999 Nov 8	IRTF	192	. . .	. . .	. . .
Par 21	1998 Jul 7	CTIO	262	1998 Jul 7	CTIO	131
Par 21	1999 Nov 12	IRTF	192	1999 Nov 12	IRTF	192

dust, SEDs that peak in the far-IR or submillimeter and spectral indices of $\alpha > 0.3$. "Flat-spectrum" sources are Class I objects that exhibit flat SEDs between 2 and 20 μm and indices between 0.3 and -0.3. Class II objects are more evolved, usually optically visible, exhibit SEDs that peak in the near-IR, with $-0.3 > \alpha > -1.6$, and lack massive circumstellar envelopes. These sources exhibit IR excesses that can be modeled by circumstellar accretion disks. Class III objects are considered to be the most evolved sources. These objects lack massive envelopes and circumstellar disks and show minimal IR excesses, with $\alpha < -1.6$. Most FU Ori objects show large IR excesses, which have been successfully modeled as Class II accretion disks (Hartmann & Kenyon 1996). However, many objects also show evidence for large circumstellar envelopes on the basis of millimeter and far-IR observations. Some authors are now suggesting that FU Ori objects may represent an evolutionary stage closer to Class I sources than to the more evolved Class II sources (Sandell & Weintraub 2001; Kenyon & Hartmann 1991).

In this paper we present near-IR (3–5 μm) and mid-IR (7–20 μm) imaging and spectroscopy of four members of the FU Ori class, RNO 1B and RNO 1C, Z CMa, and Par 21, as well as one object, V380 Ori, that has been described as a pre-FU Ori object (Welin 1987). We show SEDs and mid-IR color temperatures for all sources. We resolve multiple sources and

extended emission in the RNO 1B/C system. We discuss the properties of these sources, association with disk activity, and identify the origin of the *Infrared Astronomical Satellite* (*IRAS*) far-IR and water maser emission with a heavily embedded source in the RNO 1B/C field. These results lend strong support to the presence of disks in FU Ori systems.

2. OBSERVATIONS

The observations reported here were obtained with five different instruments: the University of Florida Observatory Spectrometer Camera for the Infrared (OSCIR), the NSFCam near-IR camera, the NASA Ames High-Efficiency Faint Object Grating Spectrometer (HIFOGS), the Aerospace Corporation's Broadband Array Spectrograph System (BASS), and the 10 m Heinrich Hertz Telescope of the Submillimeter Telescope Observatory (SMTO). Observation details are discussed below, and observing logs are shown in Tables 1, 2, and 3.

2.1. *Mid-IR Imaging*

All objects were observed at 10.8 μm ($\Delta\lambda$ FWHM $\simeq$ 5.2 μm) and 18.2 μm ($\Delta\lambda$ FWHM $\simeq$ 1.7 μm) using OSCIR, the University of Florida's 128×128 Si:As BIB array camera at the NASA Infrared Telescope Facility (IRTF) 3 m telescope and the NOAO Cerro Tololo Inter-American Observatory (CTIO)

TABLE 2
HIFOGS Observing Log

UT Date (1)	Integration (minutes) (2)	Aperture[a] (arcsec) (3)	Air-Mass Range (4)	Flux Standard (5)	Air-Mass Standard (6)	Scaling Factor (7)	Phot.[b] (%) (8)
			V380 Ori				
1992 Feb 24...........	25	10.5	1.28–1.30	α Tau	1.12	1.17	3
1992 Feb 25...........	30	10.5	1.30–1.31	α Tau	1.12	1.10	7
1992 Oct 17	50	10.5	1.30–1.42	α Tau	1.05	1.00	10
1992 Oct 26	20	10.5	1.30–1.33	α Tau	1.29	1.02	10[c]
			Z CMa				
1994 Oct 21	12	7.0	1.39–1.40	α Tau	1.23	. . .	10[d]

[a] Aperture diameter was 1.5 mm in 1992 and was reduced to 1.0 mm in 1994 by means of improved focal plane guiding techniques.
[b] Photometric reproducibility of standard stars: the fractional deviation of the ratio of a star to itself from unity.
[c] Very stable sky all night. Excellent photometry (4%) at beginning of the night was degraded to 10% because of problems with the stability of chopping the secondary waveform.
[d] Aperture alignment poor (30% loss of flux for both target and standard stars).

TABLE 3
BASS Observing Log

UT Date	Object	Air Mass	Integ. (s)
2002 Jul 27	Par 21	1.35	400
	Par 21	1.45	400
	α Lyr	1.36	200
	α Lyr	1.92	200
2002 Jul 28	RNO 1B	1.38	500
	Par 21	1.04	700
	α Lyr	1.07	200
	α Lyr	1.38	100
2002 Jul 31	RNO 1B	1.41	800
	Par 21	1.24	800
	Par 21	1.14	800
	α Lyr	1.21	300
	α Lyr	1.06	300
	α Lyr	1.11	300
	α Lyr	1.72	300
2002 Aug 1	RNO 1B	1.39	300
	α Lyr	1.19	200
	α Lyr	1.22	200
	α Lyr	1.40	200

4 m telescope. The detector has a plate scale of 0″223 pixel^{-1} and a field of view of 28″5 × 28″5 at the IRTF and a 0″183 pixel^{-1} plate scale and a 23″4 × 23″4 field of view at CTIO. Zero-magnitude fluxes and central wavelengths for the OSCIR IR photometric passbands are available in Polomski et al. (2002). The chopping secondary throw was 30″ north-south for observations at the IRTF and 23″ north-south at CTIO. Frame times were 20 ms at the IRTF and ranged between 10 and 12 ms at the CTIO. The chop frequency was ∼5 Hz for the IRTF and ∼4 Hz at CTIO. An observing log is shown in Table 1.

Flux calibration for the IRTF data was performed using the stars α Ari, γ Aql, α Mon, α CMa, and λ Vel. All standards were observed within 0.15 air masses of the science objects. Atmospheric extinction corrections were applied to all observations of the RNO 1 region. Fluxes of the calibration stars are listed in Table 4. Repeated observations of standards in the 10 and 18 μm filters suggest calibration uncertainties of 10% and 15%, respectively.

2.2. Near-IR Imaging

The RNO 1B/C region was also observed, on 2001 July 30 and 31, with broadband filters at 3.8 μm ($\Delta\lambda$ FWHM ≈ 0.076 μm) and 4.8 μm ($\Delta\lambda$ FWHM ≈ 0.23 μm) at the IRTF using the NSFCAM 256 × 256 InSb array camera (Shure et al. 1994). The 4 μm imaging was taken in tip-tilt mode to obtain a better quality point-spread function (PSF). We used the 0″148 pixel scale for a field of view of 37″9 × 37″9. Frame times were 1 s with 10 co-adds

TABLE 4
Calibration-Star Fluxes

	Flux Density (Jy)	
Name	N	18 μm
α Ari	75	25
γ Aql	72	24
α CMa.......................	131	41
α Mon	9	. . .
λ Vel..........................	196	58

and 16 cycles, for a total on-source time of 160 s at 3.8 μm and 0.0774 s, 50 co-adds, and 16 cycles, for a total on-source time of 62 s at 4.8 μm. The same time was spent alternating on a sky field 2′ south. All data were dark-subtracted and flat-fielded. Bad pixels were removed with a σ filter. Flux calibration was performed using observations of the IR standard HD 225023. We assumed an A0 spectral template (Cohen et al. 1992) normalized to the 3.8 μm flux of HD 225023 to obtain the monochromatic 3.8 and 4.8 μm standard fluxes of 0.39 and 0.26 Jy, respectively. We estimate flux uncertainties of 6% and 8% for the 3 and 4 μm observations, respectively. These uncertainties are based on repeated measurements of the standard star and photometric deviations in the flat fields.

2.3. Infrared Spectroscopy

V380 Ori and Z CMa were observed from 7.5 to 13.5 μm using HIFOGS (Witteborn et al. 1995) on the Mount Lemmon NASA 1.52 m telescope. V380 Ori was observed on two nights at two different epochs, on 1992 February 24 and 25 UT and 1992 October 17 and 26 UT. For the two V380 Ori observing epochs, two independent grating settings with a $n + \frac{1}{2}$ detector shift were acquired for Nyquist sampling of the flux spectra and to cover gaps in the wavelength coverage caused by bad detectors. Z CMa was observed only on one night, 1994 October 21 UT. The HIFOGS resolution per detector is approximately constant across the 120-element array at 0.045 μm per detector, yielding a resolving power of $R \simeq 170-300$ from $\lambda\lambda = 7.5-13.5$ μm. North-south chopper throws of 48″, 44″, and 40″ were used on the observing runs in 1992 February, 1992 October, and 1994 October, respectively. On 1994 October 21 UT, the HIFOGS aperture was not well centered, and approximately 30% loss of flux occurred for both Z CMa and the standard star α Tau, reducing the signal-to-noise ratio (S/N) from the nominal HIFOGS performance. Because of intermittent weather, a second spectrum of Z CMa was not obtained after the problem was corrected.

Flux calibrations were performed by dividing the flux density of the target star by that of α Tau and then multiplying by the flux spectrum of α Tau. The flux spectrum of α Tau was constructed from ground-based and airborne spectrophotometric measurements of α Tau relative to the primary standard star α Lyr (Cohen et al. 1996). Atmospheric corrections were applied by (1) computing the atmospheric transmission spectrum using ATRAN (Lord 1993) at the air masses of the target and standard stars, respectively, for an integrated column depth of water of 5.7 mm; (2) degrading the atmospheric transmission to the instrument resolution; (3) computing the ratio of the telluric transmission for target versus object; and (4) dividing the target's flux spectrum by the transmission ratio. The technique was verified by correcting the ratios of standard stars taken at different air masses, resulting in stellar ratios of ±5% through the water band (7.5–7.8 μm) and ±3% in the ozone band (9.4–9.8 μm). The water vapor column was verified by these computations and by the depth of the water band. The ratios of the standard stars to themselves were also used to determine the photometric accuracy of the night, taken as the fractional deviation of their flux ratios from unity.

To improve the S/N, each night's spectra of V380 Ori was degraded in spectral resolution by computing a statistically weighted average of the flux density in adjacent detectors. Then the independent degraded flux spectra were interlaced after adjusting the flux level using a scaling factor (Table 2). The spectra were all adjusted to the epoch of longest integration time on 1992 October 17 UT.

TABLE 5
Sᴀᴍᴘʟᴇ FU Oʀɪ Sᴛᴀʀs

Name	R.A. (J2000)	Decl. (J2000)	Spectral Type	Distance (pc)	A_ν	IRAS $F_{12\,\mu m}$ (Jy)
RNO 1................................	00 36 51.82	63 29 30.4[a]	F5 III[b]	850[c]	3.6[b]	. . .
RNO 1B............................	00 36 46.31	63 28 54.1[d]	F8 II[b]	850	9.2[b]	1.79:
RNO 1C............................	00 36 46.89	63 28 58.6[d]	. . .	850	12[b]	1.79:
V380 Ori...........................	05 36 25.43	−06 42 57.7[e]	B8/A1[f]	460[e]	1.5[g]	8.62
Z CMa...............................	07 03 43.15	−11 33 06.2[d]	B5/8+F5 I[h]	930[i]	2.4[e]	126.6
Par 21	19 29 00.81	09 38 46.7[d]	A5–F5 Iab[j,k]	400[g]	4.0[j]	0.76

Nᴏᴛᴇ.—Units of right ascension are hours, minutes, and seconds, and units of declination are degrees, arcminutes, and arcseconds.
[a] Average of GSC 2.2 and USNO-A1.0 coordinates.
[b] Staude & Neckel (1991).
[c] Yang et al. (1991).
[d] Sandell & Weintraub (2001).
[e] van den Ancker et al. (1998).
[f] Leinert et al. (1997).
[g] Finkenzeller & Mundt (1984).
[h] Kenyon & Hartmann (1991).
[i] Ibragimov & Shevchenko (1990).
[j] Neckel & Staude (1984).
[k] Staude & Neckel (1992).

Spectra of RNO 1B and Par 21 were obtained with BASS at the NASA IRTF on 2002 July 27, 28, 31, and August 1. BASS consists of a pair of cooled prisms that disperse the spectrum onto two 58-element blocked impurity band linear arrays that simultaneously span the $3-13.5$ μm region. The spectral resolution ranges from about 30 to 125 over each of the $3-6$ and $6.5-13.5$ μm regions. A $3''.8$ aperture was used along with a 7.1 Hz chop rate and $25''$ nod throw. Calibration was performed using the star α Lyr for which a 9700 K blackbody and 10 μm flux of 1.26×10^{-16} W cm^{-2} μm^{-1} were assumed (Lynch et al. 2001). Atmospheric extinction corrections were applied to all observations. All BASS spectral data points, such as those in the atmospheric CO$_2$ and H$_2$O bands (2.9 and $5.5-7.0$ μm), with errors exceeding the observed flux (i.e., S/N less than unity) have been rejected. An observing log is shown in Table 3.

2.4. Submillimeter Photometry

We observed Par 21 with the 870 μm 19-channel bolometer array on 2003 April 21 at the SMTO. The array consists of 19 hexagonal $22''.4$ wide detectors separated by $\approx 50''$, with a noise equivalent flux density of ≈ 0.6 Jy s$^{-1/2}$. Continuum on/off measurements were made with a nod throw of $\pm 60''$ in azimuth and a 4 Hz chop. Eight separate continuum scans were obtained, each composed of 40 subscans having on- and off-source scans of 10 s each, for a total on-source integration time of 1600 s. Submillimeter opacity was determined from sky dips at 870 μm. The observations of Par 21 were reduced with the New Imaging Concept (NIC) software package (SMTO Users Manual), corrected for atmospheric opacity, and co-added. Calibration was performed using observations of 3C 279, 3C 273, and the planet Mars.

3. SOURCES

The astrophysical parameters for all six sources are listed in Table 5. We summarize the properties of each source below.

3.1. RNO 1 Region

The RNO 1 complex (=IRAS 00338+6312) contains at least three PMS stars: RNO 1, 1B, and 1C. This region is located within the dark cloud L1287 at a distance of ~ 850 pc (Yang et al. 1991). RNO 1 is offset from RNO 1B and 1C by $50''$ in the nebula GN 00.34.0. Both RNO 1B and RNO 1C have been classified as FU Ori stars; a large 3 mag outburst was observed at the location of RNO 1B, and both sources display the characteristic CO absorption bands (Kenyon et al. 1993; Staude & Neckel 1991). RNO 1 may be a Herbig star (Staude & Neckel 1991). Two other protostellar sources, visible in the near-IR, RNO 1F and RNO 1D (Weintraub & Kastner 1993) are located within arcseconds of RNO 1B and 1C. Weintraub et al. (1996) found several near-IR polarization peaks; DLIRIM 1, DLIRIM 2, and DLIRIM 3, which indicate the positions of deeply embedded sources near RNO 1B and 1C. Sandell & Weintraub (2001) find strong submillimeter emission from multiple sources in this region. IRAS found strong mid-IR emission in this region but was unable to resolve the individual sources. The centroid of the IRAS emission is not coincident with either RNO 1B or RNO 1C, and it is uncertain which object dominates the mid-IR and far-IR fluxes.

The region is also associated with a bipolar molecular outflow, a radio continuum source with a jet, several water masers, and methanol maser emission (Fiebig et al. 1996; Wouterloot et al. 1993; Szymczak et al. 2000; Yang et al. 1991; Anglada et al. 1994). Analysis of the velocity structure of the water maser emission suggests an origin in a circumstellar disk (Fiebig et al. 1996). Finally, Graham & Chen (1991) detected a 3.1 μm ice absorption feature around RNO 1B; such a feature could be formed within a dense circumstellar disk.

3.2. V380 Ori

V380 Ori (=IRAS 05339−0644) is located within the diffuse nebula NGC 1999 at a distance of 460 pc and was initially identified as a T Tauri star by Herbig (1946). This source has been described as a pre–FU Ori star on the basis of its similarity to known FU Ori systems (Welin 1987). V380 Ori is associated with multiple Herbig-Haro objects, as well as a bipolar outflow, and is a $0''.14$ binary with a late-type companion. The primary dominates the SED at IR wavelengths (Millan-Gabet et al. 2001; Corcoran & Ray 1995; Leinert et al. 1997). Both polarimetry and photometric observations show irregular
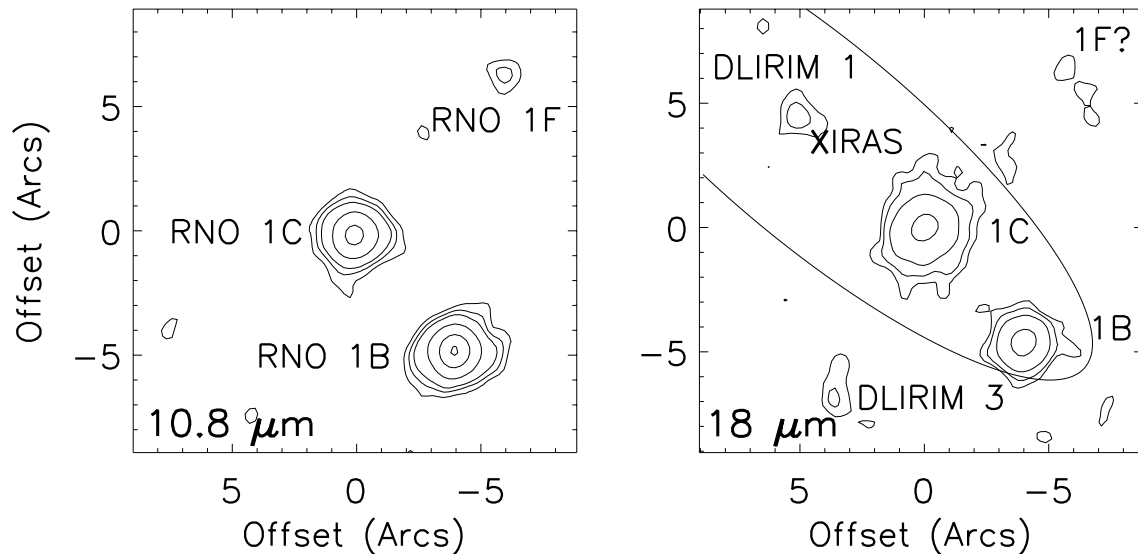
FIG. 1.—OSCIR mid-IR imaging of the RNO 1B/C region. All data has been Gaussian smoothed by 3 pixels for clarity, and the lowest contour shown is at the 3 σ level. *Left*: 10.8 μm imaging. Contour levels are 9, 18, 30, 90, 300, and 600 mJy arcsec^{-2}. *Right*: 18.2 μm imaging. Contour levels are 31.2, 52, 104, and 312 mJy arcsec^{-2}. The *IRAS* source is marked with a cross and the *IRAS* positional uncertainty ellipse is shown.

variability; however, no large (>1 mag) eruptions have been observed (Davies et al. 1990; Vrba et al. 1979; Carpenter et al. 2001). Mid-IR spectroscopy suggests a small 10 μm emission feature (Cohen & Witteborn 1985; Cohen 1973), and interferometric observations in the near-IR show a small halo $\approx$1 AU in size (Millan-Gabet et al. 2001).

3.3. *Z CMa*

Z CMa (=IRAS 07013−1128) is a luminous, close (0″.1) binary system located in a cometary nebula at a distance of 930 pc (Ibragimov & Shevchenko 1990; Leinert & Haas 1987; Koresko et al. 1991). The optically brighter source is an FU Ori star, and the IR companion may be a Herbig star (Covino et al. 1984; Koresko et al. 1991; Whitney et al. 1993; Hartmann et al. 1989). No optical outbursts have ever been detected from the Z CMa system. This unusual system has been detected at wavelengths ranging from the radio to the X-ray (Skinner et al. 1993; Zinnecker & Preibisch 1994). Z CMa is also associated with 15 Herbig-Haro objects (Poetzel et al. 1989), a bipolar CO outflow (Evans et al. 1994), extended millimeter emission (Henning et al. 1998), and a thermal jet originating from the FU Ori component (Velázquez & Rodríguez 2001). The object shows a 10 μm absorption feature (Cohen & Witteborn 1985; Olnon et al. 1986) and weak 2.3 μm CO absorption (Hartmann et al. 1989).

3.4. *Par 21*

Par 21 (=IRAS 19266+0932) is located within a highly polarized cometary nebula at a distance of $\approx$400 pc (Draper et al. 1985). Polarization maps show morphology suggestive of a circumstellar disk (Draper et al. 1985; Bastien & Ménard 1990). Par 21 was identified as an FU Ori source on the basis of observations of P Cygni profiles indicating mass loss and doubled absorption lines indicating disk rotation (Staude & Neckel 1992). No outburst has been recorded for this object, and no observations of the 2.3 μm CO feature have yet been conducted. The source is associated with a bipolar Herbig-Haro outflow, as well as several near-IR companions (Staude & Neckel 1992; Li et al. 1994). Mid-IR photometry shows a flat

energy distribution characteristic of Class I PMS objects (Cohen 1974).

4. RESULTS AND ANALYSIS

Figures 1–9 show IR imaging and spectroscopy of the program stars. We discuss the observational results for each source below.

4.1. *Infrared Imaging*

V380 Ori, Z CMa, and Par 21 show no extended emission or companions in our mid-IR images. These objects were compared with nearby point sources selected from the Positions and Proper Motions (PPM) catalog and found to be unresolved at both 10 and 18 μm.

The RNO 1B/C region was resolved into multiple sources and extended emission in the near and mid-IR (Figs. 1 and 2). We detect RNO 1B, 1C, and 1F at near and mid-IR wavelengths. RNO 1 was detected at both 10 and 18 μm but was not observed at the shorter wavelengths. DLIRIM 1, the near-IR polarization source, is a strong 3, 4, and 18 μm source but was not detected at 10 μm. This object also coincides with a strong 3.6 cm continuum source and a radio jet (Anglada et al. 1994). We also detect a new 3.8 μm source 2″.5 northwest of RNO 1C (RNO 1C-NW) and a 3 and 4 μm source 5″ northwest of RNO 1B (RNO 1B-NW). At 18 μm we identify an additional source that corresponds with the near-IR polarimetric source DLIRIM 3 (Weintraub et al. 1996). We do not detect the Weintraub et al. sources RNO 1D or DLIRIM 4 at any wavelength. In total, six sources are detected with near and mid-IR imaging, suggesting that this region is a young embedded cluster.

The pair of FU Ori stars, RNO 1B, and RNO 1C show very different profiles at 10 and 18 μm. RNO 1B is an unresolved point source in the near- and mid-IR. RNO 1C is unresolved at 3, 4, and 10 μm but shows elongated emission at 18 μm (Fig. 3) with a maximum extent of 4″ (at the 3 σ level) and P.A. $\approx$ −44°. A large-scale bipolar outflow at P.A. $\approx$ 45° is oriented nearly perpendicular to this structure (Evans et al. 1994). We estimated the source size by measuring the FWHM of RNO 1C (1″.6) and quadrature-subtracting the observed FWHM of the point source
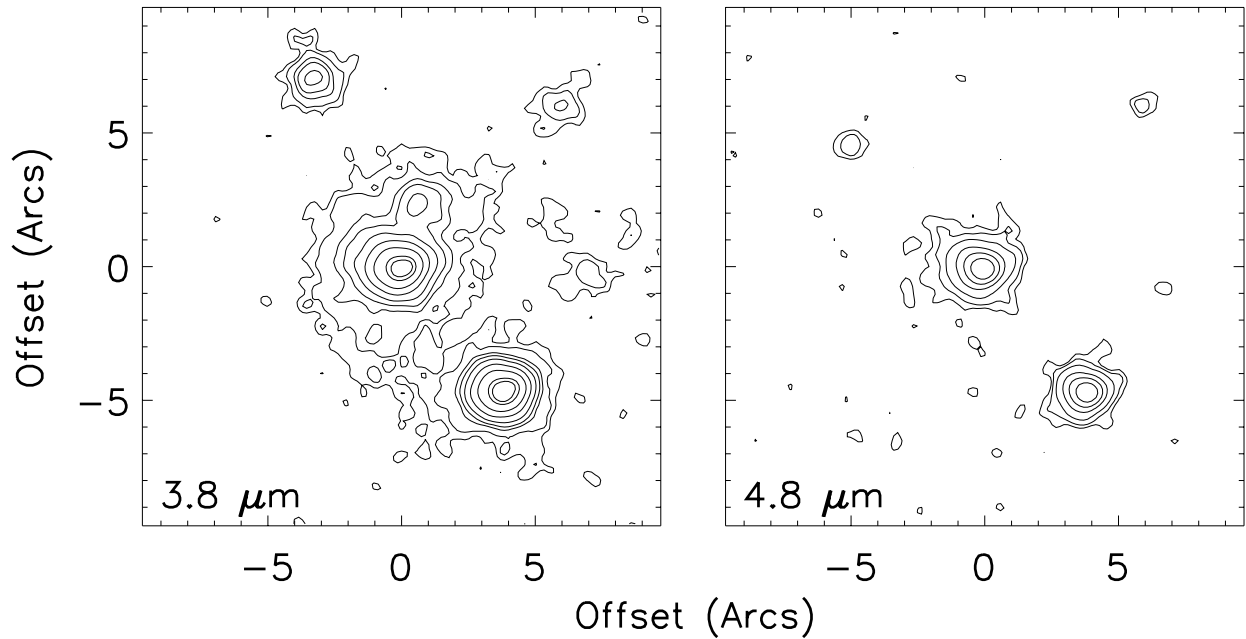
Fig. 2.—NSFCAM imaging of the RNO 1B/C region. All data has been Gaussian smoothed by 3 pixels for clarity, and the lowest contour shown is at the 3 σ level. *Left*: 3.8 μm imaging. Contour levels are 3.21, 5.35, 10.7, 16.05, 26.75, 53.5, 107, 214, and 267.5 mJy arcsec^{-2}. *Right*: 4.8 μm of the same region. Contour levels are 8.8, 14.7, 29.4, 73.5, 147, and 294 mJy arcsec^{-2}.

PPM 25578 (1″3). The angular size of the emission, $r \approx 360$ AU (assuming $d = 850$ pc), is similar to that of silhouette disks in Orion (McCaughrean & O'Dell 1996).

One of the key questions concerning this region is the source of the molecular outflow and the identity of the associated *IRAS* source. The *IRAS* Point Source Catalog (1988) (PSC) lists a mid-IR source, IRAS 00338+6312, located $\sim 40''$ southeast of RNO 1 in the vicinity of RNO 1C. Several authors have suggested that this source powers the strong bipolar molecular outflow seen in this region (Yang et al. 1991; Snell et al. 1990). However, the position of the *IRAS* source is almost 6″ offset from RNO 1C. Weintraub et al. suggest that it may instead be associated with another more deeply embedded source. Our IR images reveal several additional sources in this region that coincide with the locations of polarimetric peaks in Weintraub & Kastner's (1993) maps. In addition, near-IR imaging by Weintraub et al. (1996) shows that these peaks are associated with faint 3 μm sources.

We suggest that DLIRIM 1 is the origin of *IRAS* far-IR emission and the bipolar outflow. This object is located within 1″6 of the centroid of the *IRAS* position ellipse (Fig. 1b). DLIRIM 1 is also a strong candidate for a circumstellar disk. Multiwavelength phenomena associated with disks are detected near this source. Water masers showing Keplerian velocity signatures are found within 1″ (Fiebig et al. 1996), a radio continuum source with a jet is located with 2″ (Anglada et al. 1994), submillimeter observations show a massive dusty source in this region (Sandell & Weintraub 2001), and the IR source itself shows strong polarization (Weintraub et al. 1996) and a silicate absorption feature (this paper).

Far-IR imaging as well as high-resolution mid-IR spectroscopy will soon be available from NASA's *Spitzer Space Telescope* and may help clarify the nature of this region and reveal other deeply embedded sources.

4.2. SEDs and Photometry

Near-IR photometry of RNO 1B and 1C was conducted using an 18 pixel (2″7) radius aperture. This aperture is ≈ 3 times the FWHM of the 3.8 μm PSF and 6 times the FWHM of the 4 μm PSF. Sky emission was estimated from the median of an annulus surrounding each source. Photometry of confused regions was performed by masking out extraneous sources. We found that this method introduced an extra 3% uncertainty in the near-IR fluxes. Mid-IR photometry of all sources was conducted by growing an aperture around each object until the statistical
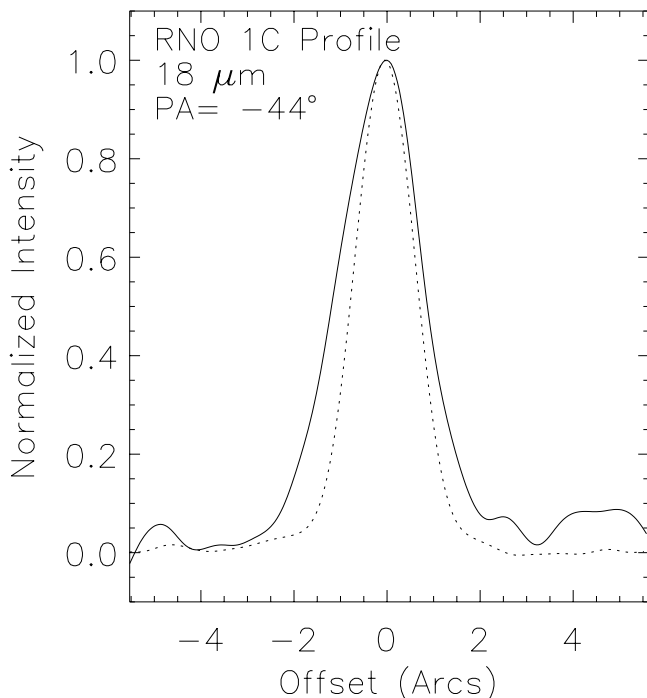

Fig. 3.—Radial profile cut at position angle $-44°$ across RNO 1C 18 μm image (*solid line*) with the same profile for the point source PPM 25578 superposed.

TABLE 6
FLUX DENSITIES (Jy)

Name	3.8 μm	4.67 μm	10.8 μm	18 μm	α[a]
RNO 1	. . .	. . .	0.52	0.97	−0.38
RNO 1B	0.68	0.58	1.24	1.61	−0.65
RNO 1C	0.78	0.67	0.79	2.34	−0.41
RNO 1F	0.03	0.02	0.08	. . .	. . .
RNO 1C-NW	0.13	. . .	. . .	. . .	. . .
DLIRIM 1	0.06	0.04	. . .	0.18	−0.30
DLIRIM 3	. . .	. . .	. . .	0.18	. . .
V380 Ori	. . .	. . .	7.97	6.64	−0.39
Z CMa......................................	. . .	. . .	121.82	151.30	−0.01
Par 21	. . .	. . .	0.96	3.43	0.74

[a] Spectral index.

noise exceeded the increase in flux. Both the mid- and near-IR photometry are presented in Table 6.

We show in Figures 4, 5, and 6 the 1–20 μm SEDs derived from our observations and from data in the literature. When possible, we selected literature data that was contemporaneous (within the same year) to limit the effects of source variability. We computed the spectral index α for each object by least-squares fitting of all data between 2.2 and 18 μm. We deliberately excluded 3.0 and 10 μm photometry, since some objects show evidence for spectral features such as ice and silicates in these regimes. Photometry and spectral indices of all the sources are presented in Table 6.

The three brightest sources in the RNO 1 region, RNO 1, 1B, and 1C all fall into the Class II category but exhibit markedly different SEDs (Fig. 4). RNO 1B and 1C show a sharp rise in flux from 1–2 μm, while RNO 1 shows a flat SED and an abrupt decline at 3 μm. RNO 1B declines in flux to 18 μm, while RNO 1C begins to rise in flux at 18 μm, possibly indicating a 10 μm silicate absorption feature. The *Midcourse Space Experiment* (*MSX*) telescope also observed the RNO 1B/C pair but was not able to resolve the individual sources (*MSX* Archive).[5] *MSX* photometry indicates a continued rise in flux toward longer wavelengths (Fig. 4).

The 10 μm absorption feature seen in both RNO 1C and DLIRIM 1's SEDs, as well as the elongated 18 μm emission from RNO 1C, supports the presence of large masses of dust around these objects. The absorption feature can be produced by obscuring dust, as can occur within a flattened envelope or edge-on disk (Cohen & Witteborn 1985)—for example, the disk of CRBR 2422.8−3423 (Thi et al. 2002).

Using the resolved 1–20 μm photometry from our observations and the literature, as well as optical observations from Staude & Neckel (1991) and the published extinctions toward RNO 1, 1B, and 1C (Table 5), we calculated the extinction-corrected luminosities of these three objects. We do not calculate the integrated luminosities of the other sources in this region (DLIRIM 1, RNO 1F, DLIRIM 3) because of the limited wavelength coverage available. We also note that Staude & Neckel (1991) do not cite an optical magnitude for RNO 1C. However, we found a faint detection within 1″0 in the USNO B1 catalog (Monet et al. 2003). After converting the photographic magnitude to the Landolt system, we derive an R magnitude of 15.6. We find optical to 20 μm luminosities of 44, 144, and 121 $L_{\odot}$ for RNO 1, 1B, and 1C, respectively. All sources are somewhat more luminous than expected for their spectral types. However, evolutionary models predict that young stellar objects should exhibit excess luminosity during their evolution onto the main sequence (see Palla 1999 for a review). The optical to 3.5 μm luminosity of the entire RNO1B/C system is ≈ 900 $L_{\odot}$, (assuming $A_{\nu} = 10.0$), in excellent agreement with results in Kenyon et al. (1993). However, this region emits substantial luminosity in the far-IR. Mookerjea et al. (1999) cite unresolved 12–200 μm fluxes for the RNO 1B/C region from *IRAS* and the Tata Institute of Fundamental Research balloon-borne telescope (TIFR). Including these fluxes in our calculations, we find an integrated luminosity for the entire system of ≈ 4300 $L_{\odot}$. Most of the luminosity in this region arises in the far-IR and potentially drives the bipolar outflow. Our mid-IR imaging (§ 4.1) shows that DLIRIM 1 is nearly coincident with the centroid of the *IRAS* position. However, several other
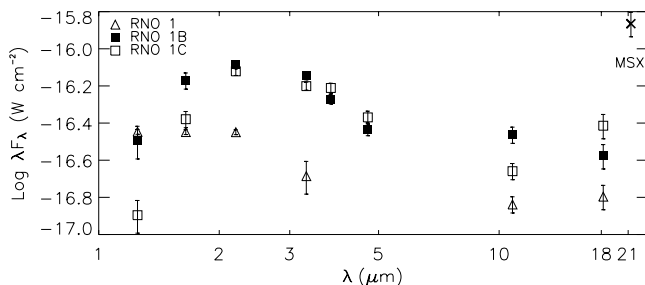
---

[5] Available at http://irsa.ipac.caltech.edu/Missions/msx.html.

FIG. 4.—The 1–20 μm SEDs of RNO1, RNO 1B, and RNO 1C. The cross indicates the 21 μm flux of the unresolved pair RNO 1B and RNO 1C from the *MSX* catalog. The 1–3 μm data are from Kenyon et al. (1993).
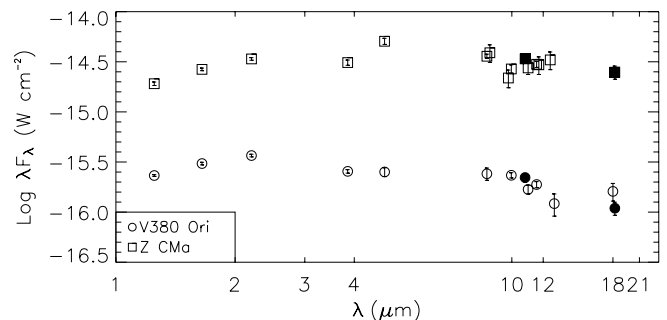

FIG. 5.—The 1–20 μm SEDs of V380 Ori and Z CMa. Filled symbols show OSCIR photometry. Other data are as follows. V380 Ori: Rossi et al. (1999), Berrilli et al. (1987), Cohen (1973), Z CMa: Teodorani et al. (1997), Berrilli et al. (1987), Persi et al. (1996).
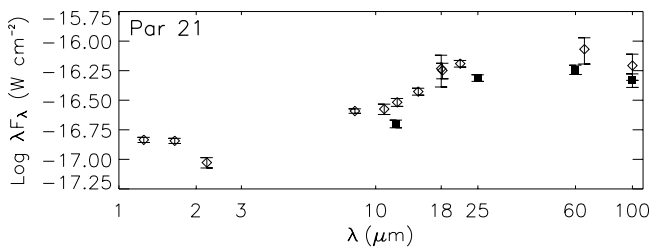
Fig. 6.—The 1–100 μm SED of Par 21. Filled squares show *IRAS* photometry. Other data are from Li et al. (1994), Cohen (1974), the *MSX* Catalog, and Ábrahám et al. (2004).

Fig. 7.—Spectroscopy of the RNO 1B/1C system with the *ISO* SWS ($R \sim 200-1000$) (*open squares*) and BASS (*circles*). The NSFCAM and OSCIR data are plotted as filled circles.

sources still lie within the *IRAS* position ellipse, and it is crucial to obtain high spatial resolution far-IR imaging to ascertain definitively which source in this region is producing the luminous far-IR emission.

These objects also show characteristics of Class I sources. The spectral indices of RNO I, RNO 1C, and DLIRIM 1 fall near the upper end of range defined for Class II objects and might better be described as Class I flat-spectrum sources. In addition, dust masses associated with submillimeter emission near the location of RNO 1C are much larger than for typical Class II objects (Sandell & Weintraub 2001), suggesting that these objects still retain massive envelopes of dust similar to those of Class I objects.

In Figures 5 and 6 we show SEDs for V380 Ori, Z CMa, and Par 21. OSCIR data are shown as filled symbols, and photometry is shown in Table 6. V380 Ori exhibits an SED that declines toward longer wavelengths, with an index characteristic of Class II sources. OSCIR mid-IR photometry for V380 Ori shows significant discrepancies with previous observations by Cohen (1973) and Berrilli et al. (1987). Extensive near-IR observations of this object have shown ~0.2 mag variability (Carpenter et al. 2001) and constrained the angular size of the emission to within 1 AU of the star (Millan-Gabet et al. 2001). In addition, we find that our 10 μm photometry is discrepant with HIFOGS spectral fluxes by almost 2 Jy, or 25%. Our observations, in conjunction with limited mid-IR monitoring by Davies et al. (1990), suggest continued variability into the mid-IR regime. Simultaneous temporal monitoring in the near- and mid-IR could help constrain the origin of the mid-IR emission. A significant lag between near- and mid-IR variation could indicate that the mid-IR emission arises in a more distant circumstellar location, such as a cool dusty envelope.

The 10 and 18 μm emission must be constrained in physical origin to 368 and 460 AU, respectively, by the width of the mid-IR PSFs (0″8 and 1″ FWHM). V380 Ori is a close binary. However, the companion cannot be the origin of the long-wavelength emission, since its SED shows a declining slope and it is likely too faint at wavelengths longer than 10 μm to be detectable (Leinert et al. 1997). Since the binary separation is at maximum 69 AU (69 sin i), the cool emission could arise in a circumbinary envelope. High spatial resolution observations with 10 m class telescopes are needed to further constrain the source of this emission.

Z CMa is a close binary, with the FU Ori object dominating the SED at visible wavelengths, while the IR range is dominated by a luminous PMS companion, which may be a Herbig Ae/Be star (Whitney et al. 1993). The Herbig star's SED is relatively flat between 2 to 20 μm with a slope $\alpha = -0.01$, which places this object in the flat-spectrum/Class I category. A slight inflection in the SED suggests a 10 μm silicate absorption feature that we confirm with mid-IR spectroscopy (§ 4.3). Z CMa is
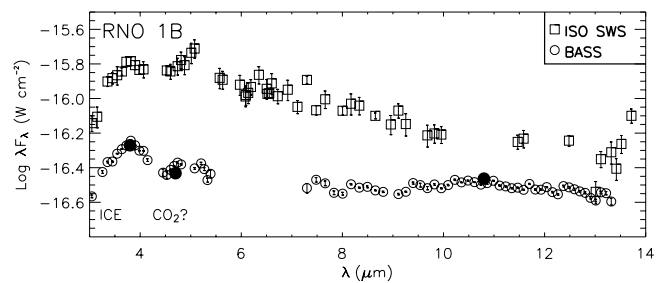
known to vary by as much as 0.3 mag in the IR, and recent observations show long-term variability in the optical and near-IR (Teodorani et al. 1997; van den Ancker et al. 2004). Our 18 μm photometry agrees well with previous observations, to within the uncertainties for each data set (Cohen 1973), but the 10 μm flux is about 25% higher than literature photometry (Berrilli et al. 1987) and 16% higher than HIFOGS 10 μm spectroscopy (§ 4.3.1). We speculate that this discrepancy could be due to variability in the strength of the silicate absorption feature. Two measurements of the 10 μm flux were made with the OSCIR detector, but they were separated by nearly a year in time; the mean flux is cited in Table 6. Both observations found fluxes more than 20% larger than previously cited fluxes (Cohen 1973; Berrilli et al. 1987).

Few observations exist in the literature for Par 21. One frequently cited *L*-band observation is only an upper limit (Cohen 1974). In Figure 6 we show all published photometry culled from the *MSX*, the *Infrared Space Observatory* (*ISO*), *IRAS*, and our own mid-IR observations spanning the 1–100 μm range (Ábrahám et al. 2004; Egan et al. 2003; PSC). The high spatial resolution, diffraction-limited OSCIR observations constrain the angular size of the Par 21 dust emission to less than 360 AU (0″9 FWHM) at 10 μm. The SED shows some indications of variability; *IRAS* photometry (*filled squares*) shows the same spectral shape but lower fluxes than the *ISO* and *MSX* photometry. The SED shows a steeply rising slope to 25 μm, with $\alpha = 0.74$, characteristic of Class I objects. At longer wavelengths the SED is relatively flat to 100 μm. We confirm this SED shape with 3–13 μm spectroscopy, for which we find $\alpha = 0.81$. The spectroscopic results are discussed further in § 4.3.

4.3. Dust Characteristics

Infrared and submillimeter photometry and spectroscopy can be used to derive dust temperatures, compositions, and masses and can help constrain the morphology of the dust emitting regions. We show in Figures 7, 8, and 9 mid-IR spectroscopy of all four sources, and we subsequently derive dust temperatures from model fits to the SEDs and spectra and dust masses from submillimeter data.

4.3.1. Spectral Features

Most FU Ori–class stars show either a weak emission feature or an absorption feature in 10 μm spectra (Hanner et al. 1998). Our new mid-IR spectroscopy of RNO 1B, V380 Ori, Z CMa, and Par 21 demonstrates a complete range of spectral phenomena, from featureless to silicate emission and silicate absorption.

The RNO 1B region was observed with the Short Wavelength Spectrometer (SWS) on *ISO*. In Figure 7 we compare the *ISO* archival spectrum (processed with On-Line Processing 10.1) with
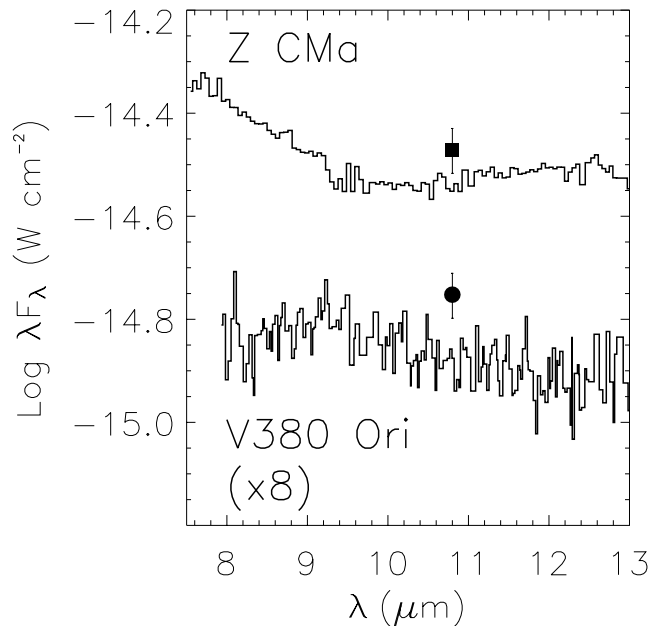
FIG. 8.—HIFOGS spectra of Z CMa and V380 Ori. V380 Ori's spectrum has been multiplied by a factor of 8. HIFOGS error bars have been omitted for clarity. OSCIR photometry for Z CMa and V380 Ori has been superposed as filled circles and squares.

FIG. 9.—BASS 3–14 μm spectroscopy of Par 21. The OSCIR, *MSX*, and *IRAS* photometry has been superposed as filled squares.

the BASS spectrum. The SWS spectrum has been rebinned to $\sim$0.1 μm resolution, and all points with uncertainties greater than 15% have been excluded. We also plotted our NSFCAM and OSCIR photometry as filled circles. BASS fluxes agree with our broadband IR photometry to within the error bars. There is agreement between the shapes of the BASS and *ISO* spectra but a factor of $\sim$3 discrepancy in the flux levels. We attribute this difference to *ISO*'s much larger aperture ($33'' \times 20''$) and to the circumstance that the emission arises in multiple sources, including the nearby IR-bright companion RNO 1C.

Both spectra show the long-wavelength edge of the 3.1 μm ice absorption feature observed by Graham & Chen (1991) and a broad feature from 4.5–5.5 μm. We suggest that this feature may arise in a blend of absorption lines from CO_2 ice at 4.27 μm and emission from hydrogen at 4.4, 4.7, and 5.1 μm (Benedettini et al. 2001). Longward of 8 μm both spectra are relatively featureless, and no obvious silicate feature is present.

In Figure 8 we show 7–13 μm HIFOGS spectra of V380 Ori and Z CMa. Data with uncertainties $\geq$15% have been excluded from the plots, and, for the sake of clarity, error bars are not shown. V380 Ori's spectrum appears relatively featureless; the small silicate emission feature seen in previous studies is absent (Cohen & Witteborn 1985). Recent studies of the T Tauri star DG Tau indicated that the silicate features of young stars can vary in strength and shape (Woodward et al. 2003), possibly because of disk activity; this scenario might apply to V380 Ori as well. Comparison of the HIFOGS spectrum with data for the same wavelength range shown in Cohen & Witteborn (1985) shows that the HIFOGS spectrum has a shallower slope, suggesting that the overall shape of the spectrum may have changed as well. Our mid-IR photometry (*filled circle*) is discrepant with the HIFOGS data, also indicating some variability.

Z CMa's spectrum shows 10 μm absorption from silicates. This feature has been present in all previous observations of Z CMa (Bhatt & Gorti 1993; Cohen & Witteborn 1985; Kraemer et al. 2002). The spectrum shows consistently lower
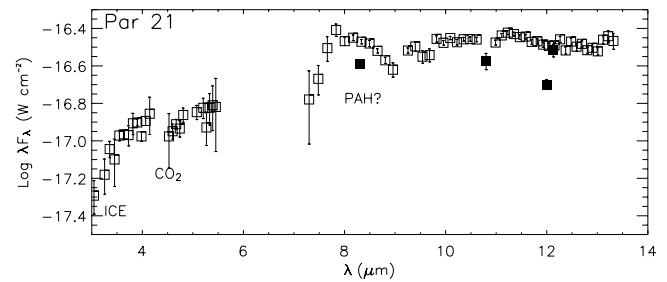
flux levels than Cohen & Witteborn (1985), as well as our own photometry (*filled square*) and may indicate some variability of the absorption feature, as discussed in § 4.2. Koresko et al. (1991) and Thiébaut et al. (1995) modeled this system's SED and found that a spherical dust envelope surrounding the Herbig star component can reproduce the silicate absorption feature.

In Figure 9 we show the first 3–14 μm spectrum of Par 21. *IRAS* (12 μm), OSCIR (10.8 μm), and *MSX* (8.3 and 12.2 μm) photometry is superposed as filled squares. The data sets show different flux levels in the 12 μm regime, suggesting some variability, as discussed in § 4.2. This object shows a wealth of spectral features from both dust and ices. Like RNO 1B, Par 21 shows water ice absorption at 3.1 μm and CO_2 ice at 4.27 μm. We interpret a strong emission feature at $\sim$8 μm as a blend of the 7.7 and 8.6 μm hydrocarbon features. Par 21 is the only FU Ori source showing hydrocarbon emission in the mid-IR. In addition, Par 21 exhibits a broad emission feature in the 9.5–12 μm regime. More evolved YSOs, such as HD 100546 (Malfait et al. 1998), sometimes exhibit emission in this regime that has been attributed to evolved silicate grains (Honda et al. 2003; Meeus et al. 2001). Models of these sources incorporate larger grains (1–2 μm) with crystalline silicate composition (Bouwman et al. 2001). Laboratory studies of crystalline silicates show emission peaking at longer wavelengths (11.2 μm) than amorphous silicate (9.7 μm), as is the case for Par 21. However, a hydrocarbon feature also occurs in the 11.3 μm regime. Considering that Par 21 shows hydrocarbon emission at 8 μm, it is likely that a small peak at 11.3 μm also originates in hydrocarbon grains. Additional emission in the 9–10.5 μm region could arise from crystalline silicates. Observations of the T Tauri star Hen 3–600A show crystalline silicate emission in this regime (Honda et al. 2003). *Spitzer* spectroscopy and imaging of Par 21 is currently scheduled (Gehrz GTO Program 124). With 10 times better spectral resolution and 1000 times increased sensitivity, *Spitzer* will be able to disentangle the multiple spectral features of Par 21 and determine their compositional origin.

4.3.2. *Dust Temperature and Optical Depth*

We used simple one-dimensional radiative transfer models of dust emission based on code written by Városi & Dwek (1999) to fit the mid-IR (7–14 μm) regime of our spectra. The shorter wavelength emission of FU Ori systems shows numerous absorption features from gas in the accretion disk atmosphere, as well as the influence of scattering processes. Detailed accretion disk models and better spectral resolution near-IR data are more appropriate to model this regime (Hartmann & Kenyon 1985). However, steady accretion disk models tend to breakdown in the mid-IR where the observed emission exceeds the model predictions (Hartmann & Kenyon 1996; Kenyon & Hartmann 1991); at these wavelengths the emission may be dominated by thermal
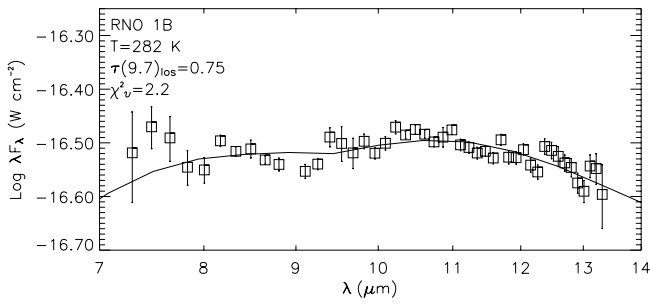
FIG. 10.—Single-temperature dust model fit to the BASS 7–14 μm spectrum of RNO 1B.

FIG. 11.—Same as Fig. 10, but for the HIFOGS 7–13 μm spectrum of V380 Ori.

emission from a dusty envelope. Simple one-dimensional modeling can still yield important information concerning grain temperature, size, and extinction toward these sources.

We tested a simple one temperature model,

$$F_\nu = \Omega\left\{\left[1 - e^{-\tau(\nu)}\right]B_\nu(T)\right\}e^{-\tau(\nu)_{\mathrm{LOS}}}, \qquad (1)$$

where F_ν is the observed flux density at frequency ν, Ω is the solid angle, $\tau(\nu)$ is the emission optical depth of the circumstellar material, $B_\nu(T)$ is the Planck function at frequency ν and temperature T, and $\tau(\nu)_{\mathrm{LOS}}$ is the absorption optical depth due to the intervening interstellar and circumstellar medium. Strong features in the BASS spectra, such as hydrocarbon emission, were excluded from these model fits.

Model input parameters include a line-of-sight (LOS) extinction A_V (and corresponding τ_{LOS}; $1.086\tau_V = A_V$) toward each object (listed in Table 5), a grain size distribution ranging from 0.001 to 1.0 μm, with a power-law exponent of -3.5, analogous to the MRN model (Mathis et al. 1977), and optical constants for astronomical silicate and graphite grains from Draine & Lee (1984) and Draine (1985). We note that Draine (1985) grain constants are based on the Trapezium emissivity profile.

The extinction toward each object, A_V, is extracted from the literature and is the total LOS extinction; i.e., interstellar and circumstellar. It is often difficult to disentangle the two contributions, and few studies cite separate values for the objects analyzed here. However, the local, circumstellar extinction likely dominates for the heavily embedded FU Ori systems.

All objects require a dual component graphite+silicate grain mixture; pure silicate grain or pure graphite grain mixtures produced lower quality fits, with $\chi^2_\nu > 5$. We therefore used the standard MRN grain mixture typical of the diffuse ISM, with a silicate/graphite grain abundance of 1.12 (Draine & Lee 1984).

We used a nonlinear least-squares Levenberg-Marquardt method to solve for three parameters: dust temperature, T, the emission optical depth at 9.7 μm, $\tau(9.7)$, and the LOS extinction in the visual and at the center of the silicate band (9.7 μm), $\tau(\nu)_{\mathrm{LOS}}$ and $\tau(\mathrm{si})_{\mathrm{LOS}}$ (Bevington & Robinson 1992). The visual optical depth $\tau(\nu)_{\mathrm{LOS}}$ is derived by using the Draine dust constants and the fact that $\tau(\mathrm{si})_{\mathrm{LOS}}/\tau(\nu)_{\mathrm{LOS}} = C_{\mathrm{si}}/C_\nu$, where C is the dust cross-section for scattering and absorption in the silicate and visual bands, respectively.

We compare our results for the extinction, A_ν [as derived from $\tau(\nu)_{\mathrm{LOS}}$] with those cited in the literature and with those derived from the relationship between silicate band optical depth and the visual extinction, $A_\nu/\tau(\mathrm{si}) = 18.5$ (Roche & Aitken 1984). We discuss the results for each object below.

BASS spectroscopy of RNO 1B was fitted between 7 and 13 μm with a single-temperature model and a silicate/graphite
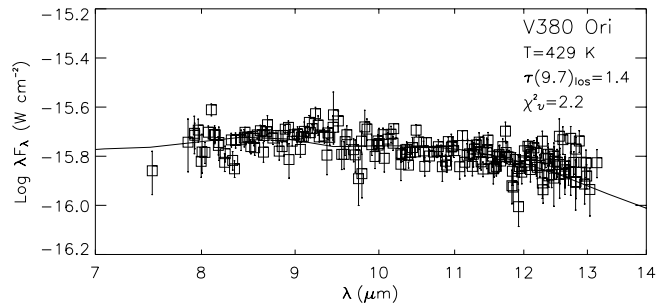
grain mixture. We found that the silicate/graphite fraction of the emission component strongly influenced the quality of the fits. Since this object shows no silicate emission, it is plausible that the dust producing the emission has a lower abundance of silicate than the standard mixture for the diffuse ISM. We therefore constructed a grid of models, varying the silicate/graphite fraction of the emission component from 0.0 to 1.0. We found the best fit (Fig. 10) $\chi^2_\nu = 2.2$, $T = 282 \pm 2$ K, $\tau(\mathrm{si})_{\mathrm{LOS}} = 0.75 \pm 0.03$, $\tau(\nu)_{\mathrm{LOS}} = 8.29 \pm 0.3$, and an emission optical depth of $\tau(9.7\ \mu\mathrm{m}) = 0.0004 \pm 0.00001$, with a silicate/graphite fraction of 0.25 for the emission component and the standard silicate/graphite fraction 1.12 for the diffuse LOS extinction component.

The visual extinction, $A_\nu = 1.086\tau_\nu$, is 9.00, in excellent agreement with published values ($A_V = 9.2$; Staude & Neckel 1991). Studies of dust in the local interstellar medium have found a relationship between silicate optical depth and extinction, $A_\nu/\tau_{\mathrm{si}} = 18.5$ (Roche & Aitken 1984). Assuming $\tau(\mathrm{si})_{\mathrm{LOS}} = 0.75$, we find $A_\nu = 13.9$, more than 4 mag fainter than published values. One possible explanation for the discrepant results is that the extinction toward RNO 1B includes a population of large grains, which produce a component of neutral extinction. Larger than normal grains have been indicated in a number of star-forming regions, for example, Orion (Cardelli & Clayton 1988), and are believed to result from grain growth processes in these regions. A study of the Taurus star formation region found anomalous values of the $A_V/\tau(\mathrm{si})$ ratio (Whittet et al. 1988), and recent studies of Herbig stars found large values of R_V, indicative of grain growth (Hernández et al. 2004).

Few data exist for RNO 1C, and the only mid-IR photometry is from our 10 and 18 μm observations. Model fits are not well constrained, and we avoid modeling this object until additional observations are available.

A comparison of V380 Ori's OSCIR photometry and HIFOGS spectrum show some variability, as discussed in § 4.2. Thus, we fitted solely the 7–13 μm spectrum. The HIFOGS spectrum is best fitted by $\chi^2_\nu = 2.2$, $T = 429 \pm 6$ K, $\tau(\nu)_{\mathrm{LOS}} = 15.7 \pm 0.4$, $\tau(\mathrm{si})_{\mathrm{LOS}} = 1.4 \pm 0.04$, and an emission optical depth of $\tau(9.7\ \mu\mathrm{m}) = 0.0007 \pm 0.00003$ (Fig. 11). We note that other authors also found temperatures in the 400–500 K range and silicate absorption optical depths ranging from 0.9 to 1.5, in good agreement with our results (Cohen & Witteborn 1985; Berrilli et al. 1992).

The visual extinction, as derived from $A_\nu = 1.086\tau_\nu$, is 17.1; greatly discrepant with published values (1.4; van den Ancker et al. 1998). In addition, assuming the relation between silicate optical depth and extinction ($A_\nu = 18.5\tau_{\mathrm{si}}$), we find a visual extinction of 25.9 mag. Several observations hint at potential problems with the visual extinction. The inherent spectral type
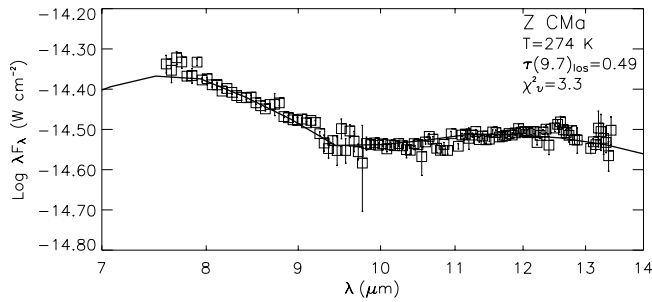
Fig. 12.—Same as Fig. 11, but for Z CMa.

Fig. 13.—Single temperature dust model fit to the BASS 7–14 μm spectrum of Par 21. Data points used in model fitting are plotted as filled squares. Excluded points are plotted as open squares.

and therefore color excess of V380 Ori are greatly uncertain. A study by Hernández et al. (2004) found that V380 Ori could not be assigned a spectral type, since it is highly veiled and does not show any photospheric absorption features. Strom et al. (1989) found values of A_V ranging from 3 to 24, depending on the method of calculation. Polarization measurements in the optical also suggest that there could be a significant contribution from scattered light at these wavelengths, and the extinction derived from optical data may be an underestimate (Jain et al. 1990). Finally, a detailed spectroscopic study of this object and the local ISM in the UV and optical also found discrepant values of the color excess, possibly due to an anomalous interstellar extinction law (Rossi et al. 1999). More detailed study of this object and its spectroscopic and photometric variability is required to disentangle contributions from scattered light and to verify the spectral type, color excess, and extinction.

Recent monitoring campaigns have shown that Z CMa varies greatly in brightness in both the optical and infrared (van den Ancker et al. 2004). Therefore, we fitted solely the simultaneous 7–14 μm HIFOGS spectroscopy with the astronomical silicate and graphite model. We also assume that the emission at these wavelengths is dominated by a single component of this binary system, the luminous Herbig Ae/Be companion. Both the SED and spectra of Z CMa show an absorption feature at ~9.7 μm attributed to silicate dust. The Draine & Lee dust model, with 1.12 silicate/graphite abundance, did not produce a good fit to this data; χ^2_ν was in excess of 9.0. Therefore, we calculated a grid of models, varying the silicate composition of both the LOS dust producing the extinction and the composition of the emitting dust. The best fit to the 7–14 μm spectrum was achieved with pure astronomical silicate dust absorption in the LOS and featureless underlying continuum emission from graphite grains (Fig. 12). This model yields $\tau(\nu)_{LOS} = 2.1 \pm 0.03$, $\tau(\mathrm{si})_{LOS} = 0.49 \pm 0.007$, an emission optical depth of $\tau(9.7\ \mu m) = 0.035 \pm 0.0004$, $T = 274 \pm 0.5$ K, and $\chi^2_\nu = 3.3$. Other studies have found τ_{si} ranging from 0.4 to 0.7 and a dust temperature of 450 K (Berrilli et al. 1992; Cohen & Witteborn 1985). The visual extinction as derived from our model fits and $A_\nu = 1.086\tau_\nu$ is 2.3, and if we assume the canonical relationship between silicate optical depth ($\tau_{\mathrm{si}} = 0.49$) and extinction, we find $A_\nu = 9.1$.

We speculate that our much lower dust temperature and the discrepant extinction results may be related to the large variations in optical and infrared brightness of this source that may have changed the slope of the SED. Recent work by van den Ancker et al. (2004) estimated the optical magnitude of the Herbig star component of this system at three epochs between 1987 and 2000, identified a flare of the Herbig star, and suggested a link with variable circumstellar extinction. Between
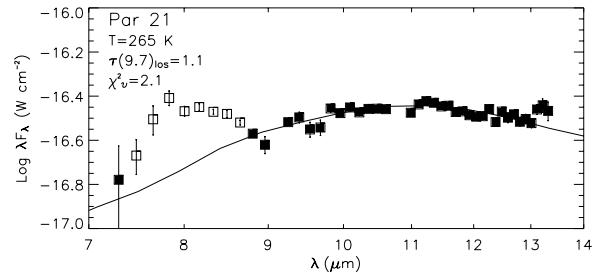
the epoch of the Cohen & Witteborn (1985) observations (1978) and the epoch of the HIFOGS observations (1994), the infrared flux increased by ≈0.3 mag, and the visual flux varied by at least a magnitude (van den Ancker et al. 2004). Extinction estimates range from 3.4 to 3.7 mag, assuming a ratio of total to selective extinction of $R = 3.1$, but it could be larger if R is larger. We note that some authors have suggested that the dust grains around very young stars are larger than those in the ISM because of grain growth processes (Pezzuto et al. 1997; Gorti & Bhatt 1993). Extinction from these larger grains might best be described by a reddening law with $R_\nu = 5$, rather than the canonical ISM $R_\nu = 3.1$ (Pezzuto et al. 1997).

The 3–14 μm BASS spectrum of Par 21 shows a wealth of features including hydrocarbon emission in the 7.5–9 μm region and additional emission at 11 μm. Limited broadband photometry also exists for Par 21; however, the SED rises steeply at 18 μm, and we found that the spectral features and the steep SED precluded good fits with our dust model. We therefore excluded the 7.5–8.7 μm emission and fitted the remainder of the 7–14 spectrum with the standard Draine & Lee silicate/graphite model (Fig. 13). We found a reasonable fit ($\chi^2_\nu = 2.1$) to the observations, with $\tau(\nu)_{LOS} = 12.1 \pm 1.0$, $\tau(\mathrm{si})_{LOS} = 1.1 \pm 0.09$, an emission optical depth of $\tau(9.7\ \mu m) = 0.0008 \pm 0.0001$, and $T = 265 \pm 9$ K. The visual extinction as derived from $A_\nu = 1.086\tau_\nu$ is 13.1 and, as derived from the optical depth of the silicate feature, $A_\nu = 20.4$.

Among all the sources examined in this study, Par 21 shows the steepest SED, implying large masses of dust at long wavelengths. In addition, the derived visual extinction of this object ($A_\nu = 13.1$) shows the greatest disagreement with published values ($A_\nu = 4.0$). Optical observations indicating large polarization of up to 40% (Draper et al. 1985), as well as our spectra showing hydrocarbon emission, suggest that the dust contains a large population of very small grains, which could indicate a strong scattered light component to the optical flux and a larger extinction than the 4.0 cited in the literature (Staude & Neckel 1992). These small grains could also influence the extinction law in this region and alter the ratio of the total to selective extinction (R). We also note the uncertain spectral type of Par 21, ranging from F5 V to A5 V and F5 Iab, which could influence previous derivations of the extinction (Neckel & Staude 1984; Staude & Neckel 1992; Hillenbrand et al. 1992). The presence of lithium in optical spectra of Par 21 also points to a later spectral type than A5 (Staude & Neckel 1992).

4.3.3. Submillimeter Dust Masses

We calculated dust masses for each object based on submillimeter photometry from the literature and our own observations of Par 21 (Table 7). We assume optically thin dust at millimeter

TABLE 7
Submillimeter Fluxes and Dust Masses

Name	λ (μm)	F_ν (mJy)	$M_{\rm dust}$ ($10^{-4} M_\odot$)	Notes
RNO 1B and 1C....................	850	6600	295.9	Sandell & Weintraub (2001)[a]
V380 Ori...............................	1300	8	0.35	Natta et al. (1997)
Z CMa..................................	850	1500	80.5	Sandell & Weintraub (2001)
Par 21	870	89	0.94	This paper

[a] RNO 1 SM1.

wavelengths with a uniform temperature of 50 K. Dust mass can be estimated from the following (Hildebrand 1983):

$$M_d = \frac{F_\nu d^2}{\kappa_\nu B_\nu(T)}, \qquad (2)$$

where F_ν is the observed flux, d is distance, $B_\nu(T)$ is the Planck function at temperature T, and κ_ν is the dust grain opacity.

Dust opacities (κ_ν) are very uncertain and can vary by a factor of 4. Natta et al. (1997) suggest a value of 1 cm^2 g^{-1} at 1300 μm, while Reipurth et al. (1993) suggest a value between 0.3 and 2.0. There is strong evidence that the value of κ_ν depends on grain size, structure, and chemical evolution (Ossenkopf & Henning 1994; Pollack et al. 1994). Older, more evolved systems, such as debris disks, may have higher values of κ_ν (Jayawardhana et al. 2002). We assume that κ_ν scales as $\kappa_\nu = \kappa_0(\lambda_0/\lambda)$ (Hildebrand 1983) and a value of $\kappa_{1300 \, \mu m} = 1$ cm^2 g^{-1}, and therefore $\kappa_{870 \, \mu m} = 1.5$. This value agrees remarkably well with theoretical values derived by Ossenkopf & Henning (1994) for very young protostars. With these simple assumptions and the distances cited in Table 5, we derive the dust masses as shown in Table 7. We note that our calculations use the full Planck function [$B_\nu(T)$]. Many authors use the Rayleigh-Jeans approximation at these wavelengths, which produces masses larger by almost a factor of 3 for our sample (Natta et al. 1997; Weintraub et al. 1991).

5. DISCUSSION

Are the observational attributes of FU Ori systems similar? Can one form a coherent picture related to their evolutionary stage and embeddedness? Multiwavelength analysis of objects in our sample leads to a confused understanding as to their relative evolutionary stages. We compare below their IR and submillimeter characteristics and discuss how these objects fit into the simple evolutionary schema for young stars.

Large submillimeter dust masses are generally accepted as indicative of youth. Younger objects, such as Class I sources, are expected to exhibit larger dust masses than more evolved objects, such as debris disk systems. SED indices can be used as a guide for relative evolutionary age. Class I sources should be younger than Class II sources. We find that Par 21, a heavily embedded Class I source, exhibits a submillimeter dust mass 300 times smaller than that of the RNO 1B/1C Class II system. However, if the dust of the Par 21 system is dominated by tiny grains, as suggested by observations of hydrocarbon emission, and large polarization, the unusually small submillimeter mass may be naturally explained. The "pre–FU Ori" system V380 Ori has the smallest dust mass and shows few of the characteristics of other FU Ori systems, such as a large optical outburst and a late spectral type. Z CMa is a special case, since the IR emission actually originates in the Herbig star component rather than the FU Ori star, and it is uncertain which component produces the submillimeter emission.

Younger sources are also expected to be more luminous in the IR, because they still retain large masses of circumstellar dust, and to exhibit more extended morphology than more evolved, and less luminous, sources. RNO 1B and RNO 1C are located within the same molecular cloud and are presumably coeval, and yet they exhibit somewhat different SEDs and mid-IR morphology. RNO 1C shows extended structure, while RNO 1B is unresolved. In addition, Par 21 has a rising, Class I SED characteristic of objects with dusty envelopes yet is unresolved in the mid-IR despite being less distant than the RNO 1B/1C system.

If one compares mid-IR spectra, most FU Ori class stars show either a weak silicate emission or absorption feature in 10 μm spectra (Hanner at al. 1998). However, unlike all other known FU Ori systems, Par 21 shows strong hydrocarbon emission, as well as possible silicate emission. The spectra of RNO 1B and V380 Ori are featureless, while broadband photometry of RNO 1C suggests a 10 μm absorption feature.

FU Ori systems are assumed to be in similar, short-lived evolutionary stages, and therefore the evolutionary stage itself should not be the mechanism determining the variation among their observational properties. The presence of 10 μm silicate emission or absorption could be influenced by disk orientation. A face-on disk would not show a strong silicate absorption feature, while an edge-on disk would show strong absorption. Models of the polarization of the Herbig star component of the Z CMa system find a disk inclination between $40°$–$60°$ (Fischer et al. 1998) suggesting that the 10 μm absorption feature could be produced in the disk. Unfortunately, it is often difficult to determine disk orientation unambiguously. Models of the optical polarization of Par 21 suggest that its disk is nearly edge-on, but no silicate absorption is apparent in its spectrum (Bastien & Ménard 1990; Draper et al. 1985). In addition, Hillenbrand et al. (1992) have successfully modeled this source's SED as originating in a face-on disk. We conclude that the presence of silicate absorption does not in itself unambiguously indicate an edge-on disk orientation.

A binary companion could also influence the observed SED. Some authors have even suggested that the FU Ori phenomenon is driven by interactions with a close companion (Reipurth & Aspin 2004). Models of binary systems predict that the tidal influence of close companions disrupt circumstellar disks and may truncate the disk beyond the orbit of the companion (Osterloh & Beckwith 1995). In this scenario the system retains less dust mass, exhibits a smaller millimeter flux, has a smaller disk radius, and therefore is less easily resolved in the IR. Both V380 Ori and Z CMa possess close ($<1''$) companions that may have influenced the distribution of dusty material in these systems. V380 Ori exhibits a smaller dust mass than any known FU Ori system by a factor of ≈ 30 (Sandell & Weintraub 2001). However, Z CMa's submillimeter dust mass is relatively large compared with most other FU Ori systems. It is still uncertain whether the submillimeter dust is circumbinary or associated primarily with the FU Ori component of this system (Sandell & Weintraub 2001).

In the face of the heterogeneity of our sample, we question what singular attributes define the FU Ori class. All the sources in our sample show evidence for molecular outflows and IR excesses, definitively placing them among the youngest PMS systems. In addition, our model fits to the silicate feature indicate an anomalous extinction law for all objects in this sample. While all of these object show some indications of variability, only RNO 1B is known to have exhibited the classic FU Ori optical eruption. Prominent CO absorption bands are also an important diagnostic criterion. These spectral features have been linked to the presence of a disk but have not been detected in other types of PMS systems (Reipurth & Aspin 1997; Calvet et al. 1991). The 2.3 μm CO absorption feature is seen in the spectra of RNO 1B, RNO 1C, and Z CMa but has not yet been explored for Par 21 and was not detected for V380 Ori (Carr 1989). In addition, a recent study by Herbig et al. (2003) suggests that the CO lines are photospheric in origin and that FU Ori outbursts might not arise in disk activity after all. Sandell & Weintraub (2001) suggest that FU Ori systems may be distinguished from other PMS stars, such as T Tauri systems, by their locations in dense molecular clouds, by the large extent of their submillimeter emission, and by their dust masses, which are typically 10 times larger than those for T Tauri systems. However, Par 21 is again an anomaly; showing one of the smallest dust masses of all these systems (Sandell & Weintraub 2001). We conclude that the IR characteristics of these systems are heavily influenced by local environmental parameters, such as grain composition, binary companions, and disk inclination.

6. SUMMARY

IR and submillimeter observations can penetrate the heavy extinction associated with the FU Ori phase of disk/star evolution and reveal the dust morphology and spectral features. We resolve a disklike structure around the FU Ori star RNO 1C for the first time and detect a cool mid-IR source, DLIRIM 1, which may be the source of additional disk activity in this region. Par 21, uniquely among all FU Ori systems, shows hydrocarbon emission, a small dust mass, and strong evidence for a large population of tiny dust grains. Z CMa is a binary system, with most of the IR emission arising in the Herbig star component, which exhibits a 10 μm silicate absorption feature. V380 Ori was tentatively classified as a pre–FU Ori system by Welin (1987). We find that it shows few of the expected features of FU Ori systems and may not actually be a member of this class. All of these objects show strong indications of extreme youth but exhibit a heterogeneous set of spectral phenomena. The IR and submillimeter emission may be influenced by disk orientation and the presence of binary companions, which could disrupt the disk.

REFERENCES

Ábrahám, P., Kóspál, Á., Csizmadia, S., Kun, M., Moór, A., & Prusti, T. 2004, A&A, 428, 89
Anglada, G., Rodriguez, L. F., Girart, J. M., Estalella, R., & Torrelles, J. M. 1994, ApJ, 420, L91
Bastien, P., & Ménard, F. 1990, ApJ, 364, 232
Benedettini, M., Pezzuto, S., Giannini, T., Lorenzetti, D., & Nisini, B. 2001, A&A, 379, 557
Berrilli, F., Corciulo, G., Ingrosso, G., Lorenzetti, D., Nisini, B., & Strafella, F. 1992, ApJ, 398, 254
Berrilli, F., Lorenzetti, D., Saraceno, P., & Strafella, F. 1987, MNRAS, 228, 833
Bevington, P. R., & Robinson, D. K. 1992, Data Reduction and Error Analysis for the Physical Sciences (Boston: McGraw-Hill)
Bhatt, H. C., & Gorti, U. 1993, Bull. Astron. Soc. India, 21, 541
Bouwman, J., Meeus, G., de Koter, A., Hony, S., Dominik, C., & Waters, L. B. F. M. 2001, A&A, 375, 950
Cardelli, J. A., & Clayton, G. C. 1988, AJ, 95, 516
Calvet, N., Hartmann, L., & Kenyon, S. J. 1991, ApJ, 383, 752
Carpenter, J. M., Hillenbrand, L. A., & Skrutskie, M. F. 2001, AJ, 121, 3160
Carr, J. S. 1989, ApJ, 345, 522
Cohen, M. 1973, MNRAS, 161, 105
———. 1974, PASP, 86, 813
Cohen, M., Walker, R. G., Barlow, M. J., & Deacon, J. R. 1992, AJ, 104, 1650
Cohen, M., & Witteborn, F. C. 1985, ApJ, 294, 345
Cohen, M., Witteborn, F. C., Carbon, D. F., Davies, J. K., Wooden, D. H., & Bregman, J. D. 1996, AJ, 112, 2274
Corcoran, D., & Ray, T. P. 1995, A&A, 301, 729
Covino, E., Terranegra, L., Vittone, A. A., & Russo, G. 1984, AJ, 89, 1868
Davies, J. K., Evans, A., Bode, M. F., & Whittet, D. C. B. 1990, MNRAS, 247, 517
Draine, B. T. 1985, ApJS, 57, 587
Draine, B. T., & Lee, H. M. 1984, ApJ, 285, 89

Draper, P. W., Warren-Smith, R. F., & Scarrott, S. M. 1985, MNRAS, 212, 1P
Egan, M. P., et al. 2003, The Midcourse Space Experiment Point Source Catalog, Version 2.3 (Tech. Rep. AFRL-VS-TR-2003-1589) (Hanscom AFB, MA: Air Force Res. Lab.)
Evans, N. J., II, Balkum, S., Levreault, R. M., Hartmann, L., & Kenyon, S. 1994, ApJ, 424, 793
Fiebig, D., Duschl, W. J., Menten, K. M., & Tscharnuter, W. M. 1996, A&A, 310, 199
Finkenzeller, U., & Mundt, R. 1984, A&AS, 55, 109
Fischer, O., Stecklum, B., & Leinert, C. 1998, A&A, 334, 969
Gorti, U., & Bhatt, H. C. 1993, A&A, 270, 426
Graham, J. A., & Chen, W. P. 1991, BAAS, 23, 1374
Greene, T. P., Wilking, B. A., Andre, P., Young, E. T., & Lada, C. J. 1994, ApJ, 434, 614
Hanner, M. S., Brooke, T. Y., & Tokunaga, A. T. 1998, ApJ, 502, 871
Hartmann, L., & Kenyon, S. 1996, ARA&A, 34, 207
Hartmann, L., & Kenyon, S. J. 1985, ApJ, 299, 462
Hartmann, L., Kenyon, S. J., Hewett, R., Edwards, S., Strom, K. M., Strom, S. E., & Stauffer, J. R. 1989, ApJ, 338, 1001
Henning, T., Burkert, A., Launhardt, R., Leinert, C., & Stecklum, B. 1998, A&A, 336, 565
Herbig, G. H. 1946, PASP, 58, 163
———. 1966, Vistas Astron., 8, 109
———. 1977, ApJ, 217, 693
Herbig, G. H., Petrov, P. P., & Duemmler, R. 2003, ApJ, 595, 384
Hernández, J., Calvet, N., Briceño, C., Hartmann, L., & Berlind, P. 2004, AJ, 127, 1682
Hildebrand, R. H. 1983, QJRAS, 24, 267
Hillenbrand, L. A., Strom, S. E., Vrba, F. J., & Keene, J. 1992, ApJ, 397, 613
Honda, M., Kataza, H., Okamoto, Y. K., Miyata, T., Yamashita, T., Sako, S., Takubo, S., & Onaka, T. 2003, ApJ, 585, L59

Ibragimov, M. A., & Shevchenko, V. S. 1990, in Classical Be Stars and Ae/Be Herbig Stars, ed. A. Kh. Mamatkazina (Alma Ata)

Jain, S. K., Bhatt, H. C., & Sagar, R. 1990, A&AS, 83, 237

Jayawardhana, R., Holland, W. S., Kalas, P., Greaves, J. S., Dent, W. R. F., Wyatt, M. C., & Marcy, G. W. 2002, ApJ, 570, L93

Joint *IRAS* Science Working Group, 1988, *IRAS* Point Source Catalog (Washington: GPO) (PSC)

Kenyon, S. J., & Hartmann, L. W. 1991, ApJ, 383, 664

Kenyon, S. J., Hartmann, L., Gomez, M., Carr, J. S., & Tokunaga, A. 1993, AJ, 105, 1505

Koresko, C. D., Beckwith, S. V. W., Ghez, A. M., Matthews, K., & Neugebauer, G. 1991, AJ, 102, 2073

Kraemer, K. E., Sloan, G. C., Price, S. D., & Walker, H. J. 2002, ApJS, 140, 389

Lada, C. J. 1987, in IAU Symp. 115, Star Forming Regions, ed. M. Pembert & J. Jugakuy (Dordrecht: Reidel), 1

Leinert, C., & Haas, M. 1987, A&A, 182, L47

Leinert, C., Richichi, A., & Haas, M. 1997, A&A, 318, 472

Li, W., Evans, N. J., II, Harvey, P. M., & Colome, C. 1994, ApJ, 433, 199

Lord, S. D. 1993, NASA Technical Report (TM-103957) (Moffet Field: NASA/ Ames Research Center)

Lynch, D. K., Russell, R. W., & Sitko, M. L. 2001, AJ, 122, 3313

Malfait, K., Waelkens, C., Waters, L. B. F. M., Vandenbussche, B., Huygen, E., & de Graauw, M. S. 1998, A&A, 332, L25

Mathis, J. S., Rumpl, W., & Nordsieck, K. H. 1977, ApJ, 217, 425

McCaughrean, M. J., & O'Dell, C. R. 1996, AJ, 111, 1977

Meeus, G., Waters, L. B. F. M., Bouwman, J., van den Ancker, M. E., Waelkens, C., & Malfait, K. 2001, A&A, 365, 476

Millan-Gabet, R., Schloerb, F. P., & Traub, W. A. 2001, ApJ, 546, 358

Monet, D. G., et al. 2003, AJ, 125, 984

Mookerjea, B., Ghosh, S. K., Karnik, A. D., Rengarajan, T. N., Tandon, S. N., & Verma, R. P. 1999, ApJ, 522, 285

Natta, A., Grinin, V. P., Mannings, V., & Ungerechts, H. 1997, ApJ, 491, 885

Neckel, T., & Staude, H. J. 1984, A&A, 131, 200

Olnon, F. M., et al. 1986, A&AS, 65, 607

Ossenkopf, V., & Henning, T. 1994, A&A, 291, 943

Osterloh, M., & Beckwith, S. V. W. 1995, ApJ, 439, 288

Palla, F. 1999, in The Origin of Stars and Planetary Systems, ed. C. J. Lada & N. D. Kylafis (Boston: Kluwer), 375

Persi, P., Busso, M., Corcione, L., Ferrari-Toniolo, M., & Marenzi, A. R. 1996, A&A, 306, 587

Pezzuto, S., Strafella, F., & Lorenzetti, D. 1997, ApJ, 485, 290

Poetzel, R., Mundt, R., & Ray, T. P. 1989, A&A, 224, L13

Pollack, J. B., Hollenbach, D., Beckwith, S., Simonelli, D. P., Roush, T., & Fong, W. 1994, ApJ, 421, 615

Polomski, E. F., Telesco, C. M., Piña, R., & Schulz, B. 2002, AJ, 124, 2207

Reipurth, B., & Aspin, C. 1997, AJ, 114, 2700

———. 2004, ApJ, 608, L65

Reipurth, B., Chini, R., Krugel, E., Kreysa, E., & Sievers, A. 1993, A&A, 273, 221

Roche, P. F., & Aitken, D. K. 1984, MNRAS, 208, 481

Rossi, C., Errico, L., Friedjung, M., Giovannelli, F., Muratorio, G., Viotti, R., & Vittone, A. 1999, A&AS, 136, 95

Sandell, G., & Weintraub, D. A. 2001, ApJS, 134, 115

Shure, M. A., Toomey, D. W., Rayner, J. T., Onaka, P. M., & Denault, A. J. 1994, Proc. SPIE, 2198, 614

Skinner, S. L., Brown, A., & Stewart, R. T. 1993, ApJS, 87, 217

Snell, R. L., Dickman, R. L., & Huang, Y.-L. 1990, ApJ, 352, 139

Staude, H. J., & Neckel, T. 1991, A&A, 244, L13

———. 1992, ApJ, 400, 556

Strom, K. M., Newton, G., Strom, S. E., Seaman, R. L., Carrasco, L., Cruz-Gonzalez, I., Serrano, A., & Grasdalen, G. L. 1989, ApJS, 71, 183

Szymczak, M., Hrynek, G., & Kus, A. J. 2000, A&AS, 143, 269

Teodorani, M., Errico, L., Vittone, A. A., Giovannelli, F., & Rossi, C. 1997, A&AS, 126, 91

Thi, W. F., Pontoppidan, K. M., van Dishoeck, E. F., Dartois, E., & d'Hendecourt, L. 2002, A&A, 394, L27

Thiébaut, E., Bouvier, J., Blazit, A., Bonneau, D., Foy, F.-C., & Foy, R. 1995, A&A, 303, 795

van den Ancker, M. E., Blondel, P. F. C., Tjin A Djie, H. R. E., Grankin, K. N., Ezhkova, O. V., Shevchenko, V. S., Guenther, E., & Acke, B. 2004, MNRAS, 349, 1516

van den Ancker, M. E., de Winter, D., & Tjin A Djie, H. R. E. 1998, A&A, 330, 145

Városi, F., & Dwek, E. 1999, ApJ, 523, 265

Velázquez, P. F., & Rodríguez, L. F. 2001, Rev. Mex. AA, 37, 261

Vrba, F. J., Schmidt, G. D., & Hintzen, P. M. 1979, ApJ, 227, 185

Wachmann, A. A. 1939, IAU Circ., 738

Weintraub, D. A., & Kastner, J. 1993, ApJ, 411, 767

Weintraub, D. A., Kastner, J. H., Gatley, I., & Merrill, K. M. 1996, ApJ, 468, L45

Weintraub, D. A., Sandell, G., & Duncan, W. D. 1991, ApJ, 382, 270

Welin, G. 1987, in IAU Symp. 122, Circumstellar Dust around FU Orionis Stars, ed. I. Appenzeller & C. Jordan (Cambridge: CfA), 67, http://adsabs. harvard.edu/cgi-bin/nph-bib_query?1987IAUS..122...67W

Whitney, B. A., Clayton, G. C., Schulte-Ladbeck, R. E., Calvet, N., Hartmann, L., & Kenyon, S. J. 1993, ApJ, 417, 687

Whittet, D. C. B., Bode, M. F., Longmore, A. J., Admason, A. J., McFadzean, A. D., Aitken, D. K., & Roche, P. F. 1988, MNRAS, 233, 321

Witteborn, F. C., Cohen, M., Bregman, J. D., Heere, K. R., Greene, T. P., & Wooden, D. H. 1995, in ASP Conf. Ser. 73, Airborne Astronomy Symposium on the Galactic Ecosystem: From Gas to Stars to Dust, ed. M. R. Haas, J. A. Davidson, & E. F. Erickson (San Francisco: ASP), 573

Woodward, C. E., et al. 2003, in ASP Conf. Ser., Debris Disks and the Formation of Planets: A Symposium in Memory of Fred Gillett, ed. L. J. Caroff & D. Backman (San Francisco: ASP), in press

Wouterloot, J. G. A., Brand, J., & Fiegle, K. 1993, A&AS, 98, 589

Yang, J., Umemoto, T., Iwata, T., & Fukui, Y. 1991, ApJ, 373, 137

Zinnecker, H., & Preibisch, T. 1994, A&A, 292, 152